Introduction to Plasmonics

Aduances and Applications

edited by

Sabine Szunerits

Rabah Boukherroub

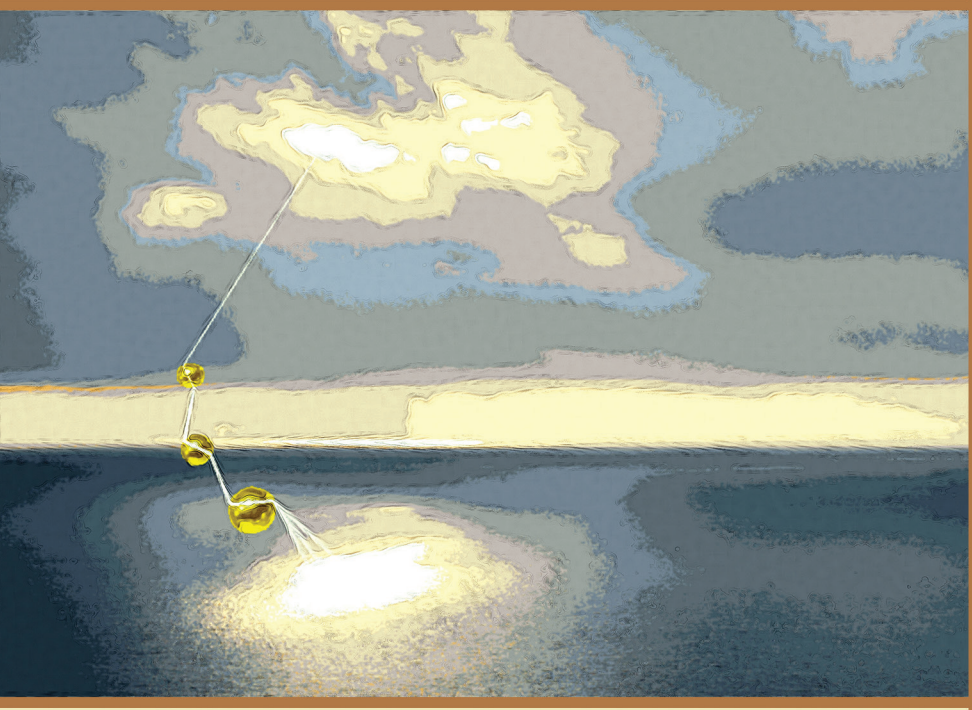

Introduction to Plasmonics

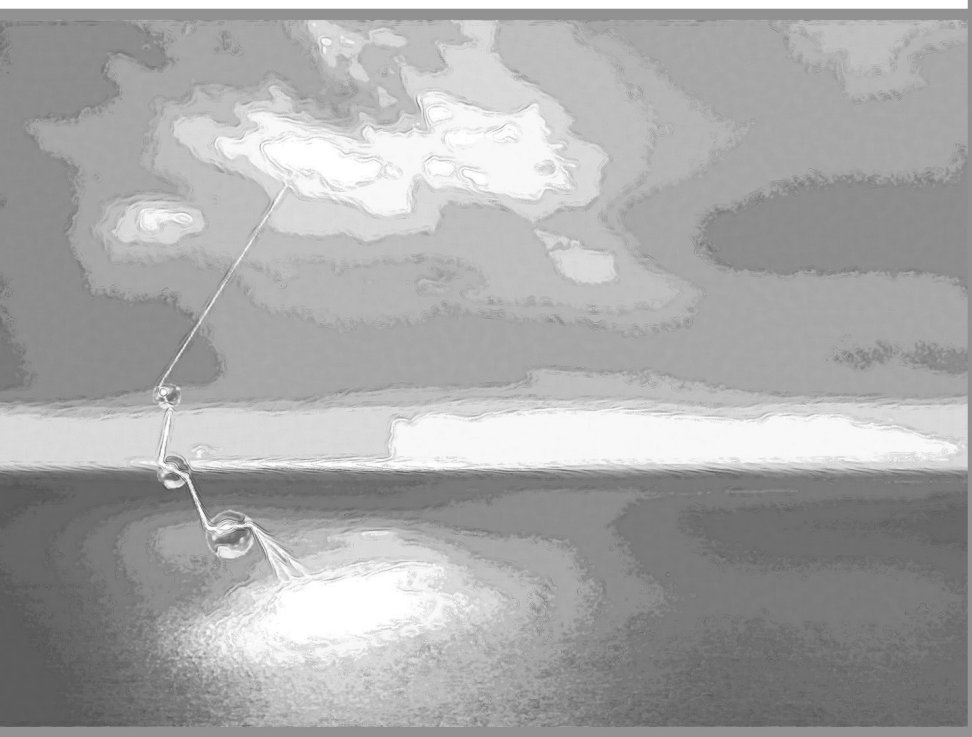

Introduction to Plasmonics

Advances and Applications

edited by

Sabine Szunerits

Rabah Boukherroub

Pan Stanford Publishing

CRC Press
Taylor & Francis Group
6000 Broken Sound Parkway NW, Suite 300
Boca Raton, FL 33487-2742

Version Date: 20150218

International Standard Book Number-13: 978-981-4613-13-2 (eBook - PDF)

Contents

Foreword

The phenomenon of surface plasmon polaritons (or surface plasmons for short) propagating as a bound electromagnetic wave, as surface light, along an interface between a (noble) metal and a dielectric medium has been known for a long time. Already in 1902, R. W. Wood, while monitoring the spectrum of (white) light after reflection by an optical (metallic) diffraction grating, noticed, "I was astounded to find that under certain conditions, the drop from maximum illumination to minimum, a drop certainly of from 10 to 1, occurred within a range of wavelengths not greater than the distance between the sodium lines" (taken from: "On a remarkable case of uneven distribution of light in a diffraction grating spectrum" *Philos. Mag.* **4**: 396). Later, this observation was understood as the first example for the optical excitation of a surface plasmon mode by light, i.e., by plane waves, reflected off the surface of a metallic grating. Various other coupling schemes using prisms to fulfill the required matching conditions between energy and momentum of surface plasmons and plane waves demonstrated a broad range of experimental configurations that allowed for the excitation of this surface light. The wavelength-dispersed direct observation of surface plasmons, excited by white light upon reflection at the metallized base of a right-angle prism as first reported by J. D. Swalen et al. ("Plasmon surface polariton dispersion by direct optical observation," *Am. J. Phys*. (1980) **48:** 670)) is shown in Figure 1. The dark curve—the "Black Rainbow"—demonstrates directly the dispersion of surface plasmons, i.e., their momentum given as the angle of resonance as a function of the excitation wavelength.

These and other experiments marked the early days of surface plasmon research aiming at elucidating the basics and potential applications, e.g., in biosensing, of these evanescent waves propagating at the interface between a mere dielectric medium and a metal that shows collective excitations of its conduction electron cloud, the plasmons. This surface light interacts with spatial (refractive index) heterogeneities at the interface in much

the same way as plane waves do, thus giving rise to the full set of optical features known from normal photons interacting with refractive index variations, like refraction, diffraction, or scattering (elastic and inelastic), and can be used for imaging purposes or for the excitation of fluorescence emission provided the chromophores are located near the interface, i.e., within the decay length of the evanescent field. Many of these aspects of surface plasmons are described in the first chapters of this book dealing with propagating surface plasmon modes.

Figure 1 The Black Rainbow.

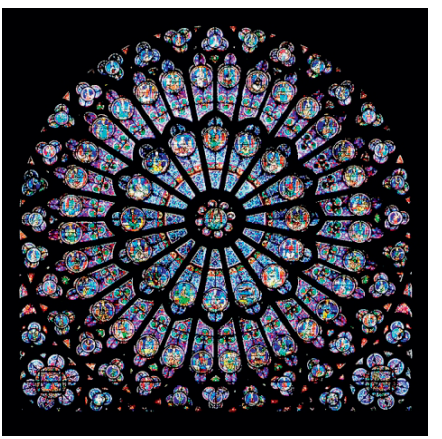

Figure 2 Gothic stained glass rose window of Notre-Dame de Paris. The colors originate from localized surface plasmons, excited in Au colloids, nanoparticles, that are embedded in the glass matrix.

More recently, another very old form of matter, i.e., colloidal gold, reinvented and renamed "Au nanoparticles," attracted a lot of interest in the context of (localized) surface plasmon excitation. Although used in stained glass for centuries (cf., e.g., the colored glass window of the cathedral Notre-Dame in Paris, shown in Figure 2) it was not until the discovery of their enormous enhancement factors seen in Raman spectroscopy or in non-linear optical spectroscopy that these nanoscopic objects became so prominent in the emerging communities of nano-scientists and nano-engineers. The obtainable optical field enhancements are well-understood as given by the resonant excitation of localized surface plasmons in particles, shells, rods, triangles, cubes, beau-ties, and a dozen other shapes of the corresponding nanoscopic resonators made from different (noble) metals. Together with a smart surface functionalization optimized for specific chemical or biological sensing platforms, this allowed for the development of spectroscopic tools, e.g., for the vibrational characterization of even single molecules or for the ultra-sensitive detection of bio-molecules from an analyte solution with an unprecedented limit of detection.

This novel class of surface plasmons in nanostructures is in the focus of the second set of chapters of the current book.

Enjoy the reading of this state-of-the-art summary of the basics and some applications of surface plasmon optics.

Wolfgang Knoll
AIT Austrian Institute of Technology
Vienna, Austria

Preface

It was in the autumn of 2002, working at the CEA (commissariat à l'énergie atomique) in Grenoble, when I became familiar with surface plasmon resonance (SPR). I had no idea that this topic would fascinate me to a point that it would become one of several common research activities with Rabah Boukherroub and finally result in the acceptance to co-edit a book on this interdisciplinary topic. The fascination around the field of plasmonics is that this topic is continuously changing and many researchers and scientists from different fields have joined the field in one way or the other.

This book presents the most widely employed plasmonic approaches and the numerous applications associated with these optical readouts. It seems that several elements underlie plasmonics research today. Advances made in nanoscience and nanotechnology have made the fabrication of plasmonic nanostructures, deposition of thin films, and development of highly sensitive optical characterization techniques possible. The different approaches to nanostructuring metals has led to a wealth of interesting optical properties and functionality via the manipulation of the plasmon modes that such structures support. The sensitivity of plasmonic structures to changes in their local dielectric environment has led to the development of new sensing strategies and systems for chemical analysis and identification.

The first part of the book deals with propagating surface plasmon resonance. Chapter 1 (by Shalabney) explores the properties, excitation, and some applications of surface plasmon polaritons on smooth and planar surfaces. Since SPR biosensors combine two building blocks, the SPR interface where the plasmonic wave is generated and an appropriate surface functionalization, it is clear that the overall performance of an SPR biosensor depends on both the intrinsic optical performance of the SPR sensor and the characteristics of the surface functionalization. Chapter 2 (by

Szunerits and Boukherroub) reviews several approaches used to impart biofunctionality to SPR interfaces and structures and hence transforming them into biosensors; a special focus was put on glycan-functionalized SPR interfaces. More recently, a third advantage was brought by the SPR imaging (SPRi) performances, which permit to follow multiple interactions in parallel. Chapter 3 (by Buhot, Pingel, Fiche, Calemczuk, and Livache) presents the SPRi apparatus and its interests for the DNA sensing and analysis.

Plasmon waveguide resonance (PWR) spectroscopy, a relatively new plasmonics-based biophysical method is presented in Chapter 4 (by Alves). Its use for the study of supported proteolipid membranes and interaction of membrane active peptides with lipid membranes is presented. Chapter 5 (by Knoll, Kasry, Huang, Wang, and Dostalek) gives an excellent insight into the race for the most sensitive platforms for biosensing applications. The chapter, entitled "Surface-Wave Enhanced Biosensing," discusses surface-plasmon field-enhanced fluorescence, long-range surface plasmon fluorescence spectroscopy, and optical waveguide fluorescence spectroscopy. This first part will be concluded by Chapter 6 (by Franzen, Losego, Kang, Sachet, and Maria) on infrared surface plasmon resonance. The state of the art of mid-infrared instrumentation and materials is discussed.

The second part of the book considers the interest of localized surface plasmons. Chapter 7 (Akjouj and Lévêque) summarizes the physical concept behind localized surface plasmon resonance. Chapter 8 (by Maurer) outlines, in a systematic manner, the different fabrication methods employed to generate plasmonic nanostructures. The use of metallic nanostructures in solution for colorimetric sensing is presented in Chapter 9 (by Aili and Sepulveda). Chapter 10 (by dos Santos, Temperini, and Brolo) follows up and describes surface-enhanced Raman scattering as means to obtain chemical information and as high sensitive detection tool. Chapter 11 (by Kocabas , Balci, and Polat) is focused on a rather novel aspect of plasmonics, graphene plasmonics. The last chapter, Chapter 12 (by Larroulet), entitled "SPR: An Industrial Point of View," rounds up the book and gives an overall conclusion.

The authors and editors of this book hope that the content will be of interest for researchers, students, and anybody interested in

the diverse aspects of plasmonics. We wish you a good time reading the chapters.

Sabine Szunerits
Rabah Boukherroub

Chapter 1

Propagating Surface Plasmon Polaritons

Atef Shalabney

ISIS, Universitè de Strasbourg and CNRS (UMR 7006),
8 allèe Gaspard Monge, 67000 Strasbourg, France

shalabney@unistra.fr

1.1 Introduction

One of the most common approaches to describe the electronic properties of the solid state is the plasma concept. In this approach, the free electrons of a metal are treated as an electron liquid of high density of about 10^{23} cm^{-3}. If one ignores the lattice in a first approximation, plasma oscillations will propagate through the metal bulk with energy quanta, called volume plasmons, of $\hbar\omega_p = \hbar\sqrt{4\pi n_e q_e^2 / m_e}$, where n_e, q_e, and m_e are the electron density, charge, and mass, respectively. This energy quanta, $\hbar\omega_p$, is of the order of few electron volts and can be excited by electron-loss spectroscopy means.

In the presence of planar boundary, there is a new mode, called surface plasmon (SP), with broad spectrum of eigen frequencies from $\omega = 0$ to $\omega = \omega_p/\sqrt{1 + \varepsilon_d}$ (ε_d—the dielectric constant of the medium adjacent to the metal) depending on the wave vector $\vec{k}$. Introducing the concept "surface plasma" in addition to the plasma

Introduction to Plasmonics: Advances and Applications
Edited by Sabine Szunerits and Rabah Boukherroub

ISBN 978-981-4613-12-5 (Hardcover), 978-981-4613-13-2 (eBook)
www.panstanford.com

concept extended the plasmon physics and opened the door for huge amount of studies in the last few decades. In an ideal semi-infinite medium, the dispersion relation of surface plasmon waves (SPW) lies to the right of the light line, which means that the SPs have longer wave vector than light waves of the same energy $h\omega$. Therefore, they are called "non-radiative" surface plasmons, i.e., they cannot decay by emitting a photon and, conversely, light incident on an ideal surface cannot excite SP.

However, under certain circumstances, SPs can couple to light-producing surface plasmon polaritons (SPPs), which their electromagnetic fields decay exponentially into the space perpendicular to the surface with maximum at the interface, as is characteristic for surface waves. From the basic dispersion relation of the SP, one can see that the increase in the momentum with respect to the light line is associated with the binding of the SP to the surface. The resulting momentum mismatch between light and SPs of the same frequency must be bridged if light is to be used to generate SPs.

There are three main techniques by which the missing momentum can be provided. The first is using a prism coupling to enhance the momentum of the incident light. The second makes use of a periodic corrugation in the metal's surface. The third involves scattering from a topological defects on the surface, such as sub-wavelength hole. The diffraction (scattering) of light by a diffraction metallic grating allows incident light to be momentum matched and thus coupled to SPs. The reverse process, importantly, allows the otherwise non-radiative SP mode to couple with light in a controlled way with good efficiency, which is vital if SP-based photonic circuits are to be developed.

This chapter is designated to explore the properties, excitation, and some applications of SPP on smooth and planar surfaces. In this case, most of the SPWs physics can be entirely understood as the picture is well mathematically defined. The second section presents the basic electrodynamics description of SPWs on planar interface in the ideal case between two semi-infinite metallic and dielectric media. In this subsection, the role of the metal optical properties will be extensively addressed with appropriate modeling of the dispersion. Although this case cannot describe the practical uses and excitations of SPP, it may provide the reader with basic

physical insights into the main properties of these waves. In the following subsections, the full dispersion relation for multilayer systems will be derived with the electromagnetic fields distribution through the layers. Two major methods of SPP excitation will be discussed in Section 1.2.4 and few applications of SPPs are discussed in Section 1.3. Our concluding remarks are briefly given in Section 1.4.

1.2 Surface Plasmons on Smooth Surfaces

Treating the optics of SPs can be done by different approaches. From the electrodynamics point of view, SPs are a particular case of surface waves, a topic that has large importance in the realm of radio-wave propagation, such as propagation along the surface of the earth. From the optics point of view, SPs are modes of an interface and from the solid-state physics point of view; SPs are collective excitation of electrons.

In this chapter, the macroscopic electrodynamics point of view will be adopted by deriving the dispersion relation of the surface wave. Within this approach, the material properties are accounted for by using a dielectric constant without any microscopic model. In order to focus on the case of SPPs, the basic Drude model will be introduced into the dispersion relation of the SP. However, the limitations of this model will be addressed, and the Lorenz–Drude model will be discussed as a good alternative in some spectral regions [1].

First, the dispersion relation of single interface bounded by semi-infinite metal and dielectric will be derived. This is the ideal case, from which one can easily understand the principles, conditions, and limitations of the SP excitation. In the next part, the practical case of multi-layer system consisting of metal slab will be addressed and different variations of this structure will be outlined. The main feature of SP waves, namely the sub wavelength confinement of the electromagnetic energy to the surface will be emphasized with its importance to different applications. The most prominent techniques of exciting SPs on smooth surfaces will be also explained.

1.2.1 Surface Plasmon at Single Interface

SP waves are a longitudinal charge density distribution generated on the metal side interface when light propagates through the metal. Both the metal and the dielectric sample can be with complex refractive indices $n_m = \sqrt{\varepsilon_m}$ and $n_d = \sqrt{\varepsilon_d}$, respectively, as shown in the inset of Fig. 1.1. Within the electrodynamics approach, the surface plasmon propagates as an electromagnetic wave parallel to the x direction with magnetic field oriented parallel to the y direction, that is, transverse magnetic polarization (TM or P) state. The condition of (TM) polarization state is needed to generate the charge distribution on the metal interface, which is considered as the first condition for SP excitation. The SP phenomenon can be easily understood, and its main characteristics can be determined by solving Maxwell's equation to the boundary-value problem.

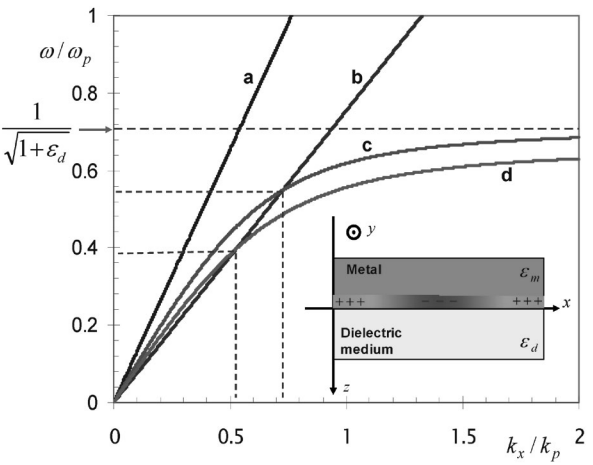

Figure 1.1 a and b show typical dispersion relation of a photon propagating in free space and inside a dielectric, respectively in order to compare with the SP dispersion. Curves c and d show the dispersion of SP at the interface between metal and dielectric. Line c corresponds to higher RI for the dielectric medium than case d. The frequency is normalized to the plasma frequency ω_p, and the x component of the light wave vector is normalized to the plasma wave number, which is defined in the text. The inset at the right bottom shows metal/dielectric interface with the coordinates system as described in the text.

In this section, we will treat the single interface case only to introduce the main features of SP waves. Hence, the full solution of the electrodynamics problem will not be detailed. In the next section, when the multi-layer system is being addressed, full description of the electromagnetic field involved in the boundary-problem will be done.

By assuming TM plane and harmonic electromagnetic fields in the metal and the dielectric sample with the appropriate waves:

$$\begin{aligned} E_i(r,t) &= (E_{ix}, 0, E_{iz}) e^{-k_{zi}|z|} e^{i(k_{xi}x-\omega t)} \\ H_i(r,t) &= (0, H_{iy}, 0) e^{-k_{zi}|z|} e^{i(k_{xi}x-\omega t)}, \end{aligned} \tag{1.1}$$

where, (i is metal, dielectric sample), k_{zi} is the z component of the wave vector in the layer i, and k_{xi} is the x component of the wave vector (or propagation constant). Substituting the fields from Eq. 1.1 into Maxwell's equations and applying the continuity conditions and the relation $k_{zi} = \sqrt{\varepsilon_i(\omega^2/c^2) - k_i^2}$ leads to

$$\begin{aligned} &\frac{k_{z1}}{\varepsilon_1} H_{1y} + \frac{k_{z2}}{\varepsilon_2} H_{2y} = 0 \\ &H_{1y} - H_{2y} = 0. \end{aligned} \tag{1.2}$$

A solution could be obtained for the last equations set by equating the determinant to zero leading to $k_{z1}\varepsilon_2 + k_{z2}\varepsilon_1 = 0$. Together with the phase-matching condition ($k_{x1} = k_{x2} = k_x$) gives an explicit expression for k_x (here $\varepsilon_m = \varepsilon_{mr} + i\varepsilon_{mi}$ and ε_d stand for ε_1 and ε_2, respectively).

$$k_x = \frac{\omega}{c} \sqrt{\frac{\varepsilon_m \varepsilon_d}{\varepsilon_m + \varepsilon_d}} \tag{1.3}$$

The value in the left hand side of Eq. (1.3) represents the surface plasmon wave vector $k_x = k_{sp}$; hence, this equation defines the dispersion relation for the propagating SP.

The requirement for surface wave imposes k_z to be pure imaginary; therefore, the term under the root of Eq. 1.3 should be larger than one, and this can be satisfied only if the two dielectric constants have opposite signs. Since in the range of

optical frequencies, the real part of the metal dielectric constant is negative ($\varepsilon_{mr} < 0$) and assuming that the dielectric medium adjacent to the metal does not or weakly absorbs in this region, the condition for SP wave (Eq. 1.3) can be fulfilled only if metallic substance possesses one of the interface sides.

In order to obtain the dispersion relation in terms of $\omega(k)$, we introduce the simplified Drude model for the metal dispersion $\varepsilon_m = 1 - \omega_p^2/\omega^2$ (ω_p is the plasma frequency given in the introduction) in Eq. (1.3) and the dispersion of the SP can be written as follows:

$$\omega^2 = \frac{1}{2}\omega_p^2 + \frac{1}{2}k_x^2c^2\left(1+\frac{1}{\varepsilon_d}\right) - \frac{1}{2}\sqrt{\omega_p^4 + 2\omega_p^2k_x^2c^2\left(1-\frac{1}{\varepsilon_a}\right) + k_x^4c^4\left(1+\frac{1}{\varepsilon_a}\right)^2} \quad (1.4)$$

One can see by the curves in Fig. 1.1 that the SP dispersion always lies to the right of the light cone (line a in the figure). However, the dispersion curve of the SP approaches the light line $\sqrt{\varepsilon_d}\omega/c$ at small k_x, it remains larger than this line so that the SPs cannot transform into light; thus, it is a nonradiative SP. At large k_x (or in case that $\varepsilon_{mr} \to -\varepsilon_d$) the value of the plasmon frequency approaches $\omega_p/\sqrt{1+\varepsilon_d}$. In this limit, the group velocity of the SP goes to zero as well as the phase velocity, so that the SP resembles localized fluctuations of the electron plasma.

It is important to emphasize that the Drude model is a crude approximation for noble metals when frequency approaches the plasma frequency. Nevertheless, this model was used in our discussion to derive the SP dispersion relation in the ideal case and to introduce few key issues for the sake of simplicity. In fact, the Drude model describes the metal optical response in the limit of zero losses where there is no damping to the free electrons oscillations inside the metal due to the electromagnetic field.

Before proceeding with the main features of SPs, it is necessary to discuss the optical properties of metals more extensively. It is important to keep in mind that although the Drude model can be very useful tool, its accuracy is much better in the IR than in the visible range. When the frequency increases, photons can excite electrons in electronic bands of lower energies so that new absorption channels are available. In addition, the Drude model cannot describe spatial dispersion and size-dependent dielectric constant. Therefore, simple phenomenological models such as the

Lorenz–Drude oscillator model based on the damped harmonic oscillator approximation can be used to describe the optical properties of metals. Here, we briefly discuss the Lorenz–Drude model often used for parameterization of the optical constants of metals.

It has been shown that the complex dielectric function $\varepsilon_m = \varepsilon_{mr} + i\varepsilon_{mi}$ can be expressed by combining the intra-band contribution, also referred to as free-electrons effect and the inter-band transitions, usually referred to as bound-electrons effect.

$$\varepsilon_m = \varepsilon_{mr} + i\varepsilon_{mi} = \varepsilon_{\text{free-electrons}} + \varepsilon_{\text{bound-electrons}} \tag{1.5}$$

The intra-band contribution (free electrons effect), $\varepsilon_{\text{free-electrons}}$, of the dielectric function is described by the same Drude model as before with introducing the damping term Γ_0, representing the losses that were not considered in the former discussion.

$$\varepsilon_{\text{free-electrons}} = 1 - \frac{f_0\omega_p^2}{\omega(\omega - i\cdot\Gamma_0)} \tag{1.6}$$

The inter-band contribution of the dielectric constant can be described, similar to the Lorenz result for insulators, as follows:

$$\varepsilon_{\text{bound-electrons}} = \sum_{j=1}^{K} \frac{f_j\omega_p^2}{(\omega_j^2 - \omega^2) + i\cdot\Gamma_j\omega}, \tag{1.7}$$

where in the last two equations ω_p is the plasma frequency and K is the number of oscillators involved with frequency ω_j strength f_j and lifetime $1/\Gamma_j$ for each oscillator

In practical use, the parameters involved in the Lorenz–Drude model are calculated by fitting to the available experimental data in the literature. The appropriate parameters for noble metals (Ag, Au, and Cu) usually used in plasmonic together with some transition metals (Ni, Ti, and Pt) can be found in Table 1.1. The parameters in Table 1.1 were mainly taken from [2].

In Fig. 1.2, the real and imaginary parts of gold and silver refractive (RI) index are shown in the range 0.5–10 μm. Silver and gold RIs are presented since these two metals are commonly used in plasmonic nanostructures due to several properties that will be discussed latter in this section and the following sections.

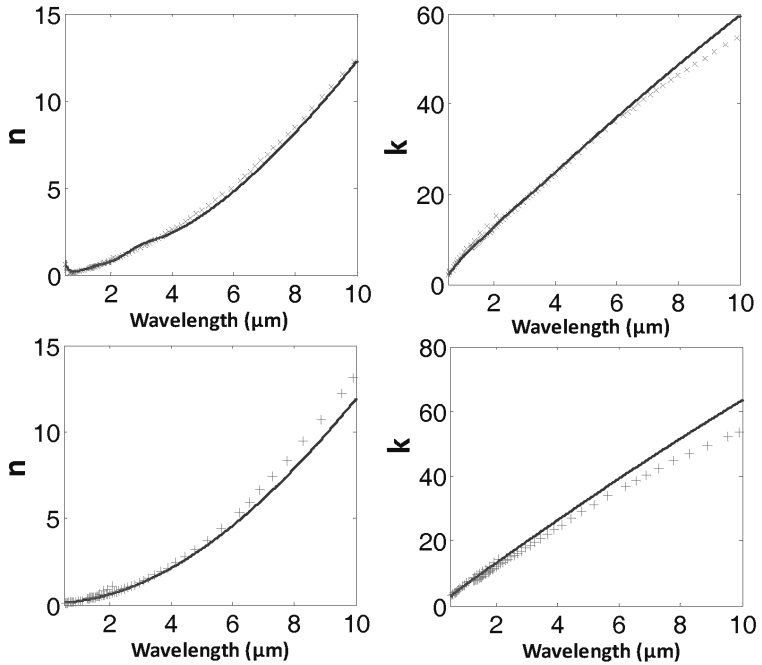

Figure 1.2 Calculated real (n) and imaginary (k) parts in solid blue lines versus experimental data in red crosses for gold (top panel) and silver (bottom panel). The parameters in table 1 were used in the calculations.

Table 1.1 Lorenz–Drude model parameters that give the best fit with the experimental data of some metals.

	Ag	Au	Cu	Ni	Ti	Pt
ω_p	9.01	9.03	10.83	15.92	7.29	9.59
f_0	0.845	0.760	0.575	0.096	0.148	0.333
Γ_0	0.048	0.053	0.030	0.048	0.082	0.080
f_1	0.065	0.024	0.061	0.1	0.899	0.191
Γ_1	3.886	0.241	0.378	4.511	2.276	0.517
ω_1	0.816	0.415	0.291	0.174	0.777	0.780
f_2	0.124	0.010	0.104	0.135	0.393	0.659
Γ_2	0.452	0.345	1.056	1.334	2.518	1.838
ω_2	4.481	0.830	2.957	0.582	1.545	1.314
f_3	0.011	0.071	0.723	0.106	0.187	0.547

Γ_3	0.065	0.870	3.213	2.178	1.663	3.668
ω_3	8.185	2.969	5.300	1.597	2.509	3.141
f_4	0.840	0.601	0.638	1.729	0.001	3.576
Γ_4	0.916	2.494	4.305	6.292	1.762	8.517
ω_4	9.083	4.304	11.18	6.089	19.43	9.249
f_5	5.646	4.384				
Γ_5	2.419	2.214				
ω_5	20.29	13.32				

Note: All values of ω_j and Γ_j are given in eV units.

Back to Eq. 1.3, one can see that in practice, the propagation constant of the SP is not purely real. The real and imaginary part of the k_{sp} can be easily derived from Eq. 1.3 by introducing the complex representation of the metal dielectric constant from Eqs. 1.5–1.7.

$$k_{x\text{–real}} = \frac{\omega}{c}\sqrt{\frac{\varepsilon_{mr}\cdot\varepsilon_d}{\varepsilon_{mr}+\varepsilon_d}}; \qquad k_{x\text{–imag}} = \frac{\omega}{c}\left(\frac{\varepsilon_{mr}\cdot\varepsilon_d}{\varepsilon_{mr}+\varepsilon_d}\right)^{3/2}\left(\frac{\varepsilon_{mi}}{2\varepsilon_{mr}^2}\right) \tag{1.8}$$

The imaginary part of the SP wave vector induces, in fact, additional damping factor parallel to the interface that originates solely from the dispersion when assuming that the dielectric medium adjacent to the metal does not absorb.

This damping factor can be quantified through the *propagation distance* L_x of the SP along the interface before damping to the half of its initial intensity; this propagation length can be expressed from the last equation as follows:

$$L_x = \frac{1}{2|k_x''|} = \frac{\lambda}{2\pi}\cdot\frac{\varepsilon_{mr}^{\ 2}}{\varepsilon_{mi}}\cdot\left[\frac{\varepsilon_a+\varepsilon_{mr}}{\varepsilon_a\cdot\varepsilon_{mr}}\right]^{3/2} \tag{1.9}$$

The damping along the interface is also combined with decay in the direction perpendicular to the interface due to the imaginary character of the z component of the wave vector (see Eq. 1.3 together with the k_z expression). The simultaneous decay of the electromagnetic fields in parallel and perpendicular to the surface extremely confines the SP to the interface as will be shown in Section 1.2.3. The decay distance, often called the *penetration*

depth of the field, can be calculated in the same manner as the propagation distance using $1/|k_z|$. The penetration inside the metal δ_m and the dielectric δ_d sides are

$$\delta_m = \frac{\lambda}{2\pi}\cdot\sqrt{\frac{\varepsilon_d+\varepsilon_{mr}}{-\varepsilon_{mr}^2}};\quad \delta_d = \frac{\lambda}{2\pi}\cdot\sqrt{\frac{\varepsilon_d+\varepsilon_{mr}}{-\varepsilon_d^2}} \tag{1.10}$$

The penetration depths presented in Eq. 1.10 correspond to the field as can be seen in Fig. 1.3 and not to the intensity; factor 1/2 should be introduced to account for the intensity damping distance.

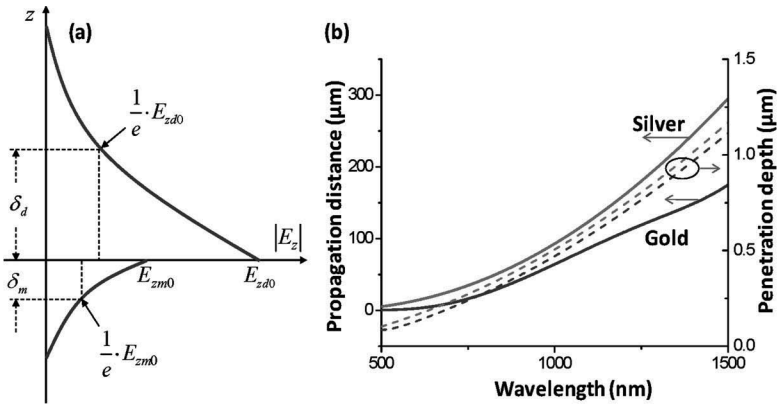

Figure 1.3 (a) Enhancing the field component perpendicular to the interface due to SPP. δ_m, δ_d, are the decay lengths of the field perpendicular to the surface in the metal and the dielectric regions, respectively (b) propagation distances (solid curves) and penetration depths (dotted curves) for gold (blue) and silver (red) for gold (silver)/air interface. The penetration depths correspond to the field intensity.

One expects that the field penetrates to larger extent inside the dielectric medium due to the smaller dielectric constant. While the penetration depths perpendicular to the interface can be sub wavelength values (tens of nanometers), the propagation distance can reach few hundreds of microns in the standard SP configurations (see Fig. 1.3).

1.2.2 Surface Plasmon in Multilayer Systems

In the previous section, the single metal/dielectric interface was only considered in order to introduce the main characteristics of SP waves generated at the interface. In real uses and experimental studies, this case is not indeed practical. In this chapter, the modes generated in a multi-layer configuration will be extensively addressed. We exploit this opportunity to introduce the full rigorous calculations, based on the electrodynamics theory to calculate the dispersion of SP supported by multi-interfaces. This rigorous treatment is arranged in top-to-bottom hierarchy. Namely, the dispersion relation will be derived for the case of two thin layers bounded by two semi-infinite media, which constitute the general case of our discussion. Simpler and more particular study cases will be then derived from the general dispersion relation.

Derivation of the dispersion relation for SPs for two adjacent thin layers with asymmetric environment:

Assume two thin layers with thicknesses a and b bounded between two semi-infinite dielectric, homogenous, and isotropic media (see Fig. 1.4). Layer (2) with thickness a and permittivity ε_2 is in the range $0 < z < a$ and layer (3) with thickness b and permittivity ε_3 extends in the range $-b < z < 0$.

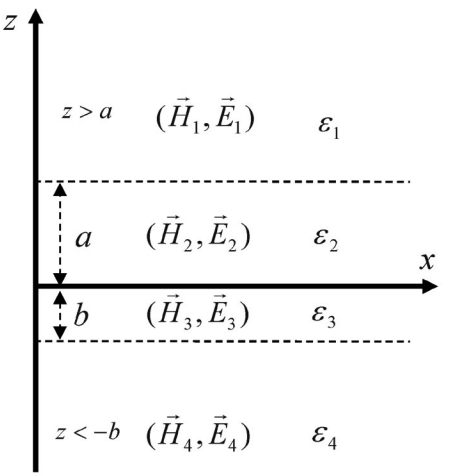

Figure 1.4 Schematic illustration of two thin layers with thicknesses a and b, and permittivities ε_2 and ε_3 bounded by two semi-infinite media with permittivities ε_1 and ε_4.

The first semi-infinite medium (medium 1) locates on the top of layer 2 with permittivity ε_1, whereas the second semi-infinite medium (medium 4) locates beneath layer 3 with permittivity ε_4.

In order to derive the dispersion relation of the entire system, p-polarized (TM) wave that propagates in the x direction is considered. The electromagnetic fields inside media i (i = 1, 2, 3, 4) that have no y dependence are of the form $\vec{H}_i$ = (0, H_{yi}, 0) and $\vec{E}_i$ = (E_{xi}, 0, E_{zi}).

Using the relations $E_{xi} = (-i/\omega\varepsilon_0\varepsilon_i)\cdot(\partial H_{yi}/\partial z)$ and $E_{zi} = (-k_x/\omega\varepsilon_0\varepsilon_i)\cdot H_{yi}$, from Maxwell equations, the fields in all regions can be written as follows:

$$
\begin{aligned}
& & H_{y1} &= A\cdot\exp i(k_x x-\omega t)\cdot\exp(ik_1 z)\\
z>a \quad & & E_{x1} &= \frac{A}{\omega\varepsilon_0}\left(\frac{k_1}{\varepsilon_1}\right)\cdot\exp i(k_x x-\omega t)\cdot\exp(ik_1 z)\\
& & E_{z1} &= \frac{-A\cdot k_x}{\omega\varepsilon_0}\left(\frac{1}{\varepsilon_1}\right)\cdot\exp i(k_x x-\omega t)\cdot\exp(ik_1 z)
\end{aligned}
\qquad (1.11)
$$

$$
\begin{aligned}
& & H_{y2} &= \exp i(k_x x-\omega t)\cdot\left[B\cdot\exp(ik_2 z)+C\cdot\exp(-ik_2 z)\right]\\
0<z<a \quad & & E_{x2} &= \frac{1}{\omega\varepsilon_0}\cdot\left(\frac{k_2}{\varepsilon_2}\right)\exp i(k_x x-\omega t)\cdot\left[B\cdot\exp(ik_2 z)-C\cdot\exp(-ik_2 z)\right]\\
& & E_{z2} &= \frac{-k_x}{\omega\varepsilon_0}\cdot\left(\frac{1}{\varepsilon_2}\right)\exp i(k_x x-\omega t)\cdot\left[B\cdot\exp(ik_2 z)+C\cdot\exp(-ik_2 z)\right]
\end{aligned}
$$

$$
\begin{aligned}
& & H_{y3} &= \exp i(k_x x-\omega t)\cdot\left[D\cdot\exp(ik_3 z)+E\cdot\exp(-ik_3 z)\right]\\
-b<z<0 \quad & & E_{x3} &= \frac{1}{\omega\varepsilon_0}\cdot\left(\frac{k_3}{\varepsilon_3}\right)\exp i(k_x x-\omega t)\cdot\left[D\cdot\exp(ik_3 z)-E\cdot\exp(-ik_3 z)\right]\\
& & E_{z3} &= \frac{-k_x}{\omega\varepsilon_0}\cdot\left(\frac{1}{\varepsilon_3}\right)\exp i(k_x x-\omega t)\cdot\left[B\cdot\exp(ik_3 z)+C\cdot\exp(-ik_3 z)\right]
\end{aligned}
$$

$$
\begin{aligned}
& & H_{y4} &= F\cdot\exp i(k_x x-\omega t)\cdot\exp(-ik_4 z)\\
z<-b \quad & & E_{x4} &= \frac{F}{\omega\varepsilon_0}\left(\frac{k_4}{\varepsilon_1}\right)\cdot\exp i(k_x x-\omega t)\cdot\exp(-ik_4 z)\\
& & E_{z4} &= \frac{-F\cdot k_x}{\omega\varepsilon_0}\left(\frac{1}{\varepsilon_4}\right)\cdot\exp i(k_x x-\omega t)\cdot\exp(-ik_4 z)
\end{aligned}
$$

The wave vector in layer *i* has the components k_x and k_i, which satisfy the relation $k_x^2 + k_i^2 = \varepsilon_i(\omega/c)^2$. The component k_z in region *i* is indicated as k_i for brevity. The continuity relations of the tangential field's components E_{xi} and H_{yi} at the three interfaces (1/2), (2/3), and (3/4) gives two linear homogenous equations for the coefficients B and C:

$$\begin{bmatrix} m_{11} & m_{12} \\ m_{21} & m_{22} \end{bmatrix} \begin{bmatrix} B \\ C \end{bmatrix} = \begin{bmatrix} 0 \\ 0 \end{bmatrix}, \quad \underline{\underline{M}} \equiv \begin{bmatrix} m_{11} & m_{12} \\ m_{21} & m_{22} \end{bmatrix} \tag{1.12}$$

The last equation, in fact, has the same form of Eq. 1.2 for the ideal interface but with new m_{ij} elements, which are as follows:

$$\begin{aligned} m_{11} &= \exp(ik_2a)\cdot\left[\varepsilon_2k_1 - \varepsilon_1k_2\right] \\ m_{12} &= \exp(-ik_2a)\cdot\left[\varepsilon_2k_1 + \varepsilon_1k_2\right] \\ m_{21} &= \exp(-ik_3b)\cdot\left[\varepsilon_3k_4 + \varepsilon_4k_3\right]\cdot\left[\varepsilon_3k_2 + \varepsilon_2k_3\right] - \exp(ik_3b)\cdot\left[\varepsilon_3k_4 - \varepsilon_4k_3\right]\cdot\left[\varepsilon_3k_2 - \varepsilon_2k_3\right] \\ m_{22} &= \exp(-ik_3b)\cdot\left[\varepsilon_3k_4 + \varepsilon_4k_3\right]\cdot\left[\varepsilon_2k_3 - \varepsilon_3k_2\right] + \exp(ik_3b)\cdot\left[\varepsilon_3k_4 - \varepsilon_4k_3\right]\cdot\left[\varepsilon_3k_2 + \varepsilon_2k_3\right] \end{aligned} \tag{1.13}$$

Using the same analogy with Eq. 1.2, in order to obtain a solution to the equation system (1.12), the determinant $\left|\underline{\underline{M}}\right|$ has to be zero. The later condition leads to the dispersion relation of the entire system described in Fig. 1.4, which is

$$\exp(2ik_2a) = \frac{-\left[1 + r_{23}\cdot r_{34}\cdot\exp(2ik_3b)\right]}{r_{12}\cdot\left[r_{34}\cdot\exp(2ik_3b) + r_{23}\right]}; \quad r_{ij} = \left(\frac{k_i}{\varepsilon_i} - \frac{k_j}{\varepsilon_j}\right) \Big/ \left(\frac{k_i}{\varepsilon_i} + \frac{k_j}{\varepsilon_j}\right) \tag{1.14}$$

One can see that the coefficients r_{ij} are, indeed, the reflection coefficients of the interface (*i*/*j*) obtained from the Fresnel equations for p-polarized light. The dispersion relation in Eq. 1.14 is the central result of this section, and will be used through all the discussion below. At this point, one should remember that dispersion relation is defined as the relation $\omega(k_x)$, which can be obtained by introducing $k_i^2 = \varepsilon_i(\omega/c)^2 - k_x^2$ into Eq. 1.14 and ending with only two dependent variables relation.

The first particular case to be discussed is the case of a single thin layer between two homogeneous semi-infinite media, which can be easily realized by setting $b = 0$ in Eq. 1.14. Actually, this gives the dispersion relation for a thin film, which was addressed in several works [3].

$$\exp(2ik_2a) = \frac{-1}{r_{12}\cdot r_{24}} = \frac{-\left(\frac{k_1}{\varepsilon_1}+\frac{k_2}{\varepsilon_2}\right)\cdot\left(\frac{k_2}{\varepsilon_2}+\frac{k_4}{\varepsilon_4}\right)}{\left(\frac{k_1}{\varepsilon_1}-\frac{k_2}{\varepsilon_2}\right)\cdot\left(\frac{k_2}{\varepsilon_2}-\frac{k_4}{\varepsilon_4}\right)} \tag{1.15}$$

One should note that the layers are numbered according to Fig. 1.4. Assuming layer 2 (with thickness a) is a metal layer, and considering the thick metal layer limit, the exponent in the left side of Eq. (1.15) vanishes and two solutions of k_x are obtained, describing two distinguished plasmons at the two metal interfaces, which are given as follows:

$$k_{x(1/2)} = \frac{\omega}{c}\cdot\sqrt{\frac{\varepsilon_1\cdot\varepsilon_2}{\varepsilon_1+\varepsilon_2}};\quad k_{x(2/4)} = \frac{\omega}{c}\cdot\sqrt{\frac{\varepsilon_2\cdot\varepsilon_4}{\varepsilon_2+\varepsilon_4}} \tag{1.16}$$

Due to the large imaginary part in the k_z inside the metal layer, the thick metal layer limit can be satisfied only by approaching the thickness a to the wavelength or even sub wavelength values. Furthermore, one can easily obtain the single interface dispersion curve that was discussed in the previous section from the last equations.

In the derivation of the dispersion relation, no restrictions were assumed on k_z. However, when SPP modes are to be derived, the lowest-order bound modes are of interest. These bounded modes only decay in the z direction and do not oscillate; therefore, the wave vectors in the z direction should be considered as pure imaginary numbers. In this case, Eq. 1.15 is valid when k_i are replaced by $i|k_i|$.

1.2.3 Electromagnetic Energy Confinement and Field Enhancement

One of the most prominent characteristic of SP waves is the confinement nature of the electromagnetic fields associated with the SP to the interface at which they are generated. Once the SP wave vector is determined by Eq. 1.14, the normalized distribution of the fields can be calculated using the equation set 1.11. Let us for simplicity, without losing the generality, assume that the magnetic field amplitude A at the 1/2 interface ($z = a$ in Fig. 1.4)

is known. In this case, one can easily express the fields' amplitudes in Eq. 1.11 as follows:

$$B = \frac{1}{2} \cdot A \cdot \exp\{i(k_1 - k_2)a\} \cdot \left[1 + \frac{k_1 \varepsilon_2}{k_2 \varepsilon_1}\right]$$

$$C = \frac{1}{2} \cdot A \cdot \exp\{i(k_1 + k_2)a\} \cdot \left[1 - \frac{k_1 \varepsilon_2}{k_2 \varepsilon_1}\right]$$

$$\begin{bmatrix} D \\ E \end{bmatrix} = \frac{1}{2} \begin{bmatrix} 1 + \frac{k_2 \varepsilon_3}{k_3 \varepsilon_2} & 1 - \frac{k_2 \varepsilon_3}{k_3 \varepsilon_2} \\ 1 - \frac{k_2 \varepsilon_3}{k_3 \varepsilon_2} & 1 + \frac{k_2 \varepsilon_3}{k_3 \varepsilon_2} \end{bmatrix} \begin{bmatrix} B \\ C \end{bmatrix}$$

$$F = D \cdot \exp\{-i(k_3 + k_4)b\} + E \cdot \exp\{i(k_3 - k_4)b\} \tag{1.17}$$

In the same manner, one can normalize all the fields in a specific system to any other component of the electromagnetic wave. As a classical example for the behavior of the fields, we consider a case in which we have two layers embedded between two semi-infinite media as depicted in Fig. 1.4. The first layer is dielectric with refractive index 1.5 and lies in the region $0 < z < 300$ nm. The second layer is made of silver with 47 nm thickness, namely located in the region $300 < z < 347$ nm. The two layers are bounded between two infinite dielectric media, with $\varepsilon_1 = 3.16$, $\varepsilon_4 = 1$ as can be seen in Fig. 1.5a. Solving the dispersion relation (1.14) for the system yields two plasmons that can be generated on the 2/3 and 3/4 interfaces: the two interfaces of the metal with the dielectric materials. Numerically, one can obtain that the plasmon at the air side (3/4 interface) propagates with $k_{sp4} = 1.02 \times 10^7$ m^{-1}, while the Plasmon at the 2/3 interface propagates with $k_{sp3} = 1.619 \times 10^7$ m^{-1}. The last values of the propagation constant of the waves are the real values of K_{sp}. From Fig. 1.5, one can see that once the plasmon is excited at the metal/air interface, the fields become to be tightly confined to this surface and rapidly decay into both the metal and the air sides. In both Figs. 1.5 and 1.6, the intensities of the electric and magnetic fields were plotted in the two thin layers and the air when $z = 0$ is set to be the first interface (1/2

interface). Figure 1.5 was obtained by substituting the first solution k_{sp4} into the fields' distribution (Eq. 1.17).

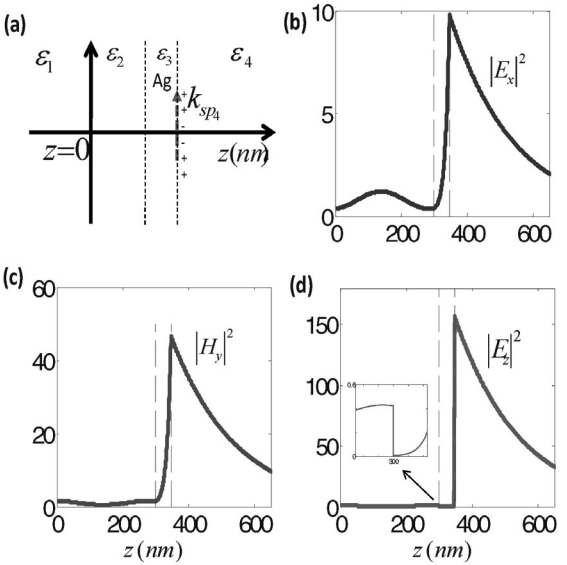

Figure 1.5 (a) Two thin layers with $\varepsilon_2 = 2.25$, $\varepsilon_3 = \varepsilon_{Ag}$ embedded between two semi-infinite media with $\varepsilon_1 = 3.16$, $\varepsilon_4 = 1$. The profiles in b, c, and d describe the intensity distributions of E_x, H_y, and E_z, respectively, for Plasmon on Ag/air interface (K_{sp4} in the text). The inset in *d* shows the discontinuity in the *Z* component of the electric field at the 2/3 interface. The wavelength is 632.8 nm and $z = 0$ is set to be the first interface (1/2 interface).

Substituting the second solution of the dispersion relation in Eq. 1.17 gives the distribution of the fields when the plasmon at the 2/3 interface is excited. These fields can be seen in Fig. 1.6.

This example was brought in order to show the fields enhancement associated with the SPP wave created on the surface. This enhancement in the fields is the key feature for the majority of plasmonics applications as will be further discussed in the following sections. However, the general structure of two layers was considered; in most of the common applications, only one thin film is located between the two media and then Eq. 1.15 should be used to calculate the propagation constant of the plasmon. In this context, a considerably interesting special case in which the

film is embedded between two symmetric media should be further discussed.

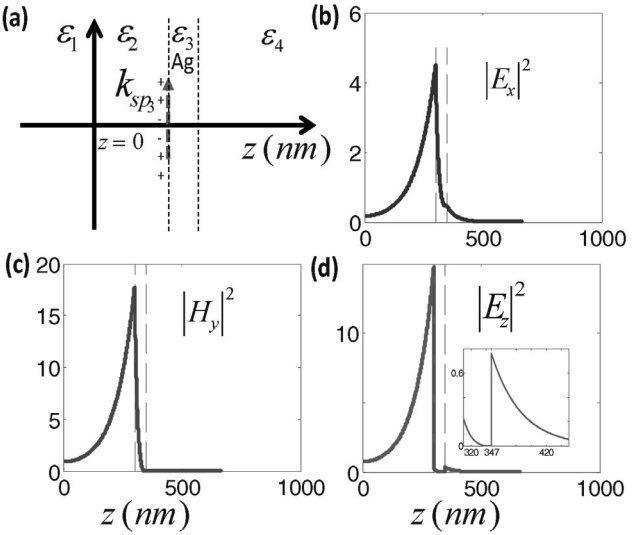

Figure 1.6 Fields distribution for the same case as in Fig. 1.5, when the second solution k_{sp3} is considered. The inset in *d* shows the discontinuity in E_Z intensity at the 3/4 interface.

When $b = 0$ and $\varepsilon_1 = \varepsilon_4 = \varepsilon_d$ in Fig. 1.4, the structure becomes symmetric by means of the dielectric response of the surrounding media and $k_1 = k_4 = k_d$. Due to the new conditions, Eq. 1.15 splits into two equations:

$$i \cdot \tan\left(\frac{k_2 \cdot a}{2}\right) = \frac{k_d \cdot \varepsilon_2}{k_2 \cdot \varepsilon_d}$$
$$i \cdot \tan\left(\frac{k_2 \cdot a}{2}\right) = \frac{k_2 \cdot \varepsilon_d}{k_d \cdot \varepsilon_2} \qquad (1.18)$$

It can be easily shown that these two dispersion relations describe two different modes that can be supported by the new system. It can be shown that the two equations in 1.18 give two different modes with odd and even parity of Ex. these two modes are of significant interest when the insulator-metal-insulator (IMI) and metal-insulator-metal (MIM) structures are considered. In the